



## Steady-state crack growth in single crystals under Mode I loading

Juul, Kristian Jørgensen; Nielsen, Kim Lau; Niordson, Christian Frithiof

*Published in:*  
Journal of the Mechanics and Physics of Solids

*Link to article, DOI:*  
[10.1016/j.jmps.2017.01.012](https://doi.org/10.1016/j.jmps.2017.01.012)

*Publication date:*  
2017

*Document Version*  
Peer reviewed version

[Link back to DTU Orbit](#)

*Citation (APA):*  
Juul, K. J., Nielsen, K. L., & Niordson, C. F. (2017). Steady-state crack growth in single crystals under Mode I loading. *Journal of the Mechanics and Physics of Solids*, 101, 209-222.  
<https://doi.org/10.1016/j.jmps.2017.01.012>

---

### General rights

Copyright and moral rights for the publications made accessible in the public portal are retained by the authors and/or other copyright owners and it is a condition of accessing publications that users recognise and abide by the legal requirements associated with these rights.

- Users may download and print one copy of any publication from the public portal for the purpose of private study or research.
- You may not further distribute the material or use it for any profit-making activity or commercial gain
- You may freely distribute the URL identifying the publication in the public portal

If you believe that this document breaches copyright please contact us providing details, and we will remove access to the work immediately and investigate your claim.

# Steady-State Crack Growth in Single Crystals under Mode I Loading

K. J. Juul\*, K. L. Nielsen, C. F. Niordson

*Department of Mechanical Engineering, Solid Mechanics, Technical University of Denmark, DK-2800 Kgs. Lyngby, Denmark*

---

## Abstract

The active plastic zone that surrounds the tip of a sharp crack growing under plane strain Mode I loading conditions at a constant velocity in a single crystal is studied. Both the characteristics of the plastic zone and its effect on the macroscopic toughness is investigated in terms of crack tip shielding due to plasticity (quantified by employing the Suo, Shih, and Varias set-up). Three single crystals (FCC, BCC, HCP) are modelled in a steady-state elastic visco-plastic framework, with emphasis on the influence rate-sensitivity and crystal structures. Distinct velocity discontinuities at the crack tip predicted by Rice [Rice J.R., 1987. Tensile crack tip fields in elastic-ideally plastic crystals. *Mech. Mater.* 6, pp. 317-335] for quasi-static crack growth are confirmed through the numerical simulations and highly refined details are revealed. Through a detailed study, it is demonstrated that the largest shielding effect develops in HCP crystals, while the lowest shielding exists for FCC crystals. Rate-sensitivity is found to affect the plastic zone size, but the characteristics overall remain similar for each individual crystal structure. An increasing rate-sensitivity at low crack velocities monotonically increases the crack tip shielding, whereas the opposite behaviour is observed at high velocities. This observation leads to the existence of a characteristic velocity at which the crack tip shielding becomes independent of the rate-sensitivity.

*Keywords:* Quasi-static crack growth, Crystal plasticity, Plastic zones, Shielding effect, Rate-sensitivity

---

\*Corresponding author

*Email address:* [krjoju@mek.dtu.dk](mailto:krjoju@mek.dtu.dk) (K. J. Juul)

---

## 1. Introduction

The active plastic zone that surrounds a crack tip has a significant influence on the fracture toughness (a composition of plastic dissipation and the work of separation), and it is the primary condition for obtaining stable crack growth. The near tip plastic zone acts as a shield against the elastic far field, which follows the well-known  $\sqrt{r}$ -singularity in the stresses, and in this way plasticity increases the toughness of the material both by dissipating energy and by lowering the near tip stress field. The active plastic zone, that surrounds the crack tip, will follow the tip during growth and create a wake of residual plastic strains as the material elastically unloads on the trailing edge. In the regions of unloading, close to the crack face, reversed plastic straining can occur. This results in continued yielding of the material, but in the opposite direction. A wide range of parameters, that describes both the material and the loading, have an influence on the development of the near tip plastic zones, and thus also on the macroscopic fracture toughness. In particular, the strain hardening of the material, governing plastic deformation, is known to influence the energy dissipation and thereby affects the energy required for the crack to advance. Thus, the strain rate hardening, that follows from rate-sensitivity, must be expected to share a similar effect on the shielding and the material toughness. The effect of the viscous behaviour was brought out in e.g. Nielsen and Niordson (2012a) for a Mode I crack travelling at steady-state in an isotropic material. Their study revealed a significant increase in the crack tip shielding for slowly growing cracks compared to a fast growing crack. Moreover, the study of Nielsen and Niordson (2012a) showed that in-between what is characterised as a slowly and a fast growing crack, a velocity leading to the rate-independent toughness can be determined.

Published studies on fracture toughness mainly considers isotropic materials (see e.g. Dean and Hutchinson, 1980; Hui, 1983; Suo et al., 1993; Tvergaard, 1997; Wei and Hutchinson, 1999; Nielsen and Niordson, 2012a). However, single crystals have been in focus due to their brittle to ductile transition temperature (see e.g. Roberts et al., 1993; Tarleton and Roberts, 2009) as-well as their distinct crack tip plastic fields (see e.g. Rice, 1987; Rice et al., 1990; Ortiz et al., 1992). Both static, quasi-static and dynamic cases ranging over both analytical and numerical calculations have been pursued.

36 The effort in these studies has been put on determining and proving the ex-  
 37 istence of specific characteristics of the material behaviour in the vicinity of  
 38 the crack tip. In single crystals, the crack tip characteristics reveal them-  
 39 selves as angular sectors separated by either stress or velocity discontinuities  
 40 (depending on whether the crack is static or growing quasi-statically). The  
 41 numerical quasi-static case performed by Rice et al. (1990) is based on a  
 42 traditional Lagrangian framework with a crack growing through a transient  
 43 phase until steady-state is achieved. Here, accepting a sparse discretization  
 44 of the domain of interest to make the computations feasible. However, this  
 45 has been improved significantly in the present study by adopting the steady-  
 46 state approach by Dean and Hutchinson (1980) which directly brings out the  
 47 field of interest and allows focusing the computational effort. Moreover, by  
 48 combining the computational framework with the SSV-model proposed by  
 49 Suo et al. (1993), a direct comparison of the crack tip shielding for various  
 50 crystal structures can be conducted in a rigorous manner.

51 The goal of the present study is to analyse quasi-static crack growth in  
 52 rate-sensitive single crystals (FCC, BCC, HCP) under Mode I loading. In  
 53 this way, the study has two parts; I) The first part is an investigation of the  
 54 characteristics of the plastic zone surrounding the crack tip for the different  
 55 crystallographic structures. This enables comparison to the work of Rice  
 56 (1987) and Rice et al. (1990), but also sheds new light on the problem as the  
 57 true steady-state is obtained within a modified boundary layer framework.  
 58 The effect of rate-sensitivity on the plastic zones will be brought out; II)  
 59 The second part of the study investigates the macroscopic crack tip shielding  
 60 under the assumption that the failure of the material is controlled by cleavage  
 61 cracking. The analysis of the shielding is based on the SSV-model by Suo  
 62 et al. (1993), which facilitates an energy based fracture criterion evaluated  
 63 by the J-integral. The effect of rate-sensitivity is of primary concern as the  
 64 viscous behaviour significantly influences the plastic field.

65 The paper is divided into the following sections: The modified bound-  
 66 ary value formulation is presented in Section 2, the material model and the  
 67 numerical formulation are presented in Section 3, validation and results are  
 68 presented in Section 4, and at last some concluding remarks are given in Sec-  
 69 tion 5. Index notation including Einstein's summation convention is used,  
 70 and the notation  $(\dot{\phantom{x}})$  signifies a time derived quantity.

## 71 2. Problem

The study is conducted under small scale yielding and treated as quasi-static i.e. the effect of inertia is neglected. A Mode I far field loading is applied on the outer boundary of the discretized material domain (illustrated in Fig. 1) according to the modified boundary layer formulation (Dean and Hutchinson, 1980), whereby the far field loading is controlled by the stress intensity factor  $K_I$

$$\sigma_{ij} = \frac{K_I}{\sqrt{2\pi r}} f_{ij}(\theta) \quad (1)$$

where  $r$  and  $\theta$  are polar coordinates related to the crack tip position and  $f_{ij}(\theta)$  are dimensionless mode functions. By introducing a reference plastic zone size parameter,  $R_0$ , depending on a reference stress intensity factor,  $K_0$ , as

$$R_0 = \left( \frac{K_0}{\tau_0} \right)^2, \quad \text{and} \quad K_0 = \sqrt{\frac{E\Gamma_{tip}}{1-\nu^2}} \quad (2)$$

72 the energy release rate at the crack tip,  $\Gamma_{tip}$  (microscopic fracture energy),  
 73 can be used as a local linear elastic fracture criterion ( $J_{tip} = \Gamma_{tip}$ ) facilitated  
 74 by modelling the SSV domain as will be described in Section 3.3. The macro-  
 75 scopic fracture energy,  $J_{ss}$ , is related to the stress intensity factor  $K_I$ , applied  
 76 at the boundary (see Fig. 1), through a relation similar to Eq. (2).

77 The crack growth problem is analysed in the 2D plane strain steady-  
 78 state framework suggested by Dean and Hutchinson (1980), whereby the  
 79 crack propagates at a constant velocity,  $\dot{a}$ . The numerical procedure iterates  
 80 directly on the stationary condition where the stress and strain field becomes  
 81 constant to an observer that follows the crack tip.

82 The 2D plane strain case is of special interest as these studies allow for  
 83 detailed experimental investigations (see e.g. Kysar et al., 2005; Dahlberg  
 84 et al., 2014). In order to analyse a material with a 3D crystallographic  
 85 structure in a 2D plane strain setting, it is necessary to invoke effective slip  
 86 systems by combining the out-of-plane slip systems to equivalent in plane  
 87 slip systems (particularly for the FCC and BCC structures). A description  
 88 of the effective slip systems can be found in Section 2.1.

89 The single crystal structures investigated belongs to the three families  
 90 most commonly found in metals; the face centered cubic (FCC), the body

centered cubic (BCC), and the hexagonal close packed (HCP). It should be mentioned, however, that cleavage cracking is not equally likely in all crystal structures. It is rather unlikely for cleavage to occur in an FCC crystal since ample slip systems for ductile behaviour exist at all temperatures for this particular crystal structure. At low temperatures, cleavage can occur in BCC crystal as only a limited number of active slip systems exist. Cleavage is also likely to be observed in HCP crystals as few slip systems are active (Anderson, 2005).

Since the material model is based on an elastic visco-plasticity theory, a definition of the active plastic zone that engulfs the crack tip is required. The quantity utilized in the present work is based on the absolute value of the accumulated slip rate,  $\dot{\Lambda} = \sum_{\alpha} |\dot{\gamma}^{(\alpha)}|$ , as suggested by Rice et al. (1990). The material properties adopted for the study can be found in Tab. 1.

### 2.1. Effective Slip Systems

To create a 2D plane strain deformation of the single crystals specific orientations are required, such that any out of plane action from one slip system are cancelled by one or more other slip systems (see e.g. Rice, 1987; Kysar et al., 2005; Niordson and Kysar, 2014). By considering the symmetry plane ( $\bar{1}01$ ) for plane strain deformation in FCC and BCC crystals, crystallographic slip systems can be combined pairwise into equivalent so-called effective slip systems where the pair is activated equally with respect to the slip such that out-of-plane actions cancel out. In FCC crystals, three such effective slip systems exist which are denoted ( $\alpha$ ), while the two crystallographic slip systems combined into each effective slip system are denoted ( $\alpha a$ ) and ( $\alpha b$ ). This can be envisioned by for example having an equal amount of slip on the (111) plane in the  $[1\bar{1}0]$  and  $[0\bar{1}1]$  direction (see fig. 2) which effectively corresponds to slip in the  $[1\bar{2}1]$  direction. For BCC crystals, only one effective slip system is constructed as the other crystallographic slip systems are already in the plane of interest. This effective slip system is constructed from Fig. 2 by having an equal amount of slip on the (101) plane in the  $[\bar{1}\bar{1}1]$  and  $[1\bar{1}\bar{1}]$  direction corresponding to slip in the  $[0\bar{2}0]$  direction. For an HCP crystal, oriented such that the basal plane (0001) is in the plane of the deformation, no effective slip systems are needed and existing prismatic crystallographic slip systems are modelled directly. The parameters and method for determining the effective slip systems are adopted from Rice (1987) and Niordson and Kysar (2014). Table 2 presents the individual crystallographic slip systems, the corresponding effective slip systems, and the crack orientation used in the

analysis (also illustrated in Fig. 3). In Tab. 2,  $\beta^{(\alpha)}$  is the effective parameter, describing the relation between the slip on the crystallographic slip systems and the corresponding effective slip system, ensuring equivalent deformation. The parameter  $\lambda^{(\alpha)}$ , gives the relation between the resolved shear stress on the crystallographic slip systems and the corresponding effective slip system. The scaling of the resolved shear stress and slip, when utilizing the effective systems, can thereby be expressed as the initial slip resistance,  $\tau_0$ , and the reference strain rate,  $\dot{\gamma}_0$ , multiplied by  $\lambda^{(\alpha)}$  and  $\beta^{(\alpha)}$  (see Tab. 2 for specific values), respectively. Hence, each effective slip system will have its own value of the slip resistance and reference strain rate according to

$$\tau_0^{(\alpha)} = \lambda^{(\alpha)} \tau_0, \quad \text{and} \quad \dot{\gamma}_0^{(\alpha)} = \beta^{(\alpha)} \dot{\gamma}_0. \quad (3)$$

As will be shown from the numerical results (see Section 4), the added corrections to the individual effective slip systems severely influence the appearance of the plastic zone that travels with the propagating crack tip.

### 3. Numerical Framework

#### 3.1. Rate-sensitive Material Model

A small strain formulation is employed where the total strain,  $\varepsilon_{ij}$ , is determined from the displacement, such that  $\varepsilon_{ij} = (u_{i,j} + u_{j,i})/2$ , which is decomposed into an elastic part,  $\varepsilon_{ij}^e$ , and a plastic part,  $\varepsilon_{ij}^p$  ( $\varepsilon_{ij} = \varepsilon_{ij}^e + \varepsilon_{ij}^p$ ). Based on the strain field, the stress field is determined from the elastic relationship;  $\sigma_{ij} = \mathcal{L}_{ijkl}(\varepsilon_{kl} - \varepsilon_{kl}^p)$ , where  $\mathcal{L}_{ijkl}$  is the elastic stiffness tensor. The total plastic strain rate,  $\dot{\varepsilon}_{ij}^p$ , in a single crystal is determined by summation over all slip systems,  $\alpha$ , according to

$$\dot{\varepsilon}_{ij}^p = \sum_{\alpha} \dot{\gamma}^{(\alpha)} P_{ij}^{(\alpha)}, \quad P_{ij}^{(\alpha)} = \frac{1}{2} \left( s_i^{(\alpha)} m_j^{(\alpha)} + m_i^{(\alpha)} s_j^{(\alpha)} \right) \quad (4)$$

where  $P_{ij}^{(\alpha)}$  is the Schmid orientation tensor,  $\dot{\gamma}^{(\alpha)}$  is the slip rate on a specific slip system, and  $s_i^{(\alpha)}$  and  $m_i^{(\alpha)}$  are two unit vectors defining the slip direction and the slip plane normal, respectively (see Fig. 3). The slip rate on each slip system,  $\alpha$ , is based on the visco-plastic power law slip rate relation proposed

by Hutchinson (1976)

$$\dot{\gamma}^{(\alpha)} = \dot{\gamma}_0 \text{sgn} \left( \tau^{(\alpha)} \right) \left( \frac{|\tau^{(\alpha)}|}{g^{(\alpha)}} \right)^{1/m} \quad (5)$$

where  $\tau^{(\alpha)} = \sigma_{ij} m_i^{(\alpha)} s_j^{(\alpha)}$  is the resolved shear stress and  $g^{(\alpha)}$  is the slip resistance evolving during plastic straining (the elasticity is assumed isotropic i.e. effects of elastic anisotropy are ignored). The relationship between the slip resistance,  $g^{(\alpha)}$ , and the plastic straining is given by the power law relation;  $g^{(\alpha)} = \tau_0 (1 + G |\gamma_{acc}^{(\alpha)}| / \tau_0)^N$ , where  $G$  is the shear modulus and  $\gamma_{acc}^{(\alpha)} = \int |\dot{\gamma}^{(\alpha)}| dt$  is the accumulated slip on slip system  $(\alpha)$ . It is evident from the slip resistance function that only self-hardening is considered in this study i.e. the hardening on a slip system is solely a result of slip on the system itself. Latent hardening, where slip on one system can affect another system, is neglected for simplicity. Furthermore, the role of twinning, which may be of importance in some metals (e.g. Mg and TiAl alloys), is not treated, however, for a more comprehensive study of these specific alloys the effect should be included.

According to Eq. (5), the rate-sensitivity of the material response increases as the rate-sensitivity exponent,  $m$ , increases and vice versa. This also implies that for  $m \rightarrow 0$ , the constitutive material model approach the response of the rate-independent material.

### 3.2. Steady-State Approach

The present study analyses the plastic zone that surrounds the tip of a sharp cleavage crack, growing at constant velocity, to bring out its effect on the material toughness (the shielding ratio). In doing so, a steady-state framework is an ideal choice as it directly brings out details on the crack tip conditions in a frame translating with the moving crack tip. In addition, the numerics also have the benefit of avoiding to explicitly model the transient period from crack initiation to steady-state growth. The steady-state finite element model employed in the present study is based on the early work of Dean and Hutchinson (1980). The steady-state condition for a continuously growing crack is described as the condition where the field quantities that surrounds the crack tip remains unchanged relative to an observer located at the crack tip. The steady-state condition states that any time derived quantity,  $\dot{f}$ , in the constitutive model can be related to a spatial derivative



174 through the velocity,  $\dot{a}$ , along a streamline, according to the relation  $\dot{f} =$   
175  $-\dot{a}\partial f/\partial x_1$  (the minus sign is due to material flow in the negative  $x_1$ -direction  
176 as illustrated in Fig. 1). Thus, any incremental quantity at a given material  
177 point  $(x_1^*, x_2^*)$ , can be evaluated by integrating along a streamline, starting  
178 upstream in the elastic zone well in front of the crack tip  $(x_1^0, x_2^*)$  and ending  
179 at the point of interest downstream  $(x_1^*, x_2^*)$  (see e.g. Juul et al., 2017). The  
180 point of interest  $(x_1^*, x_2^*)$  will then contain the load history of all upstream  
181 points. The streamline integration procedure is performed with a classical  
182 forward Euler integration scheme.

183 In the adopted steady-state framework, the displacement field,  $u_i$ , is de-  
184 termined based on the conventional principle of virtual work (PWV) for  
185 quasi-static problems

$$\int_V \mathcal{L}_{ijkl} \varepsilon_{kl} \delta \varepsilon_{ij} dV = \int_S T_i \delta u_i dS + \int_V \mathcal{L}_{ijkl} \varepsilon_{kl}^p \delta \varepsilon_{ij} dV \quad (6)$$

186 where  $T_i = \sigma_{ij} n_j$  is the surface traction. The volume analysed is denoted  $V$ ,  
187 and  $S$  is the bounding surface, with  $n_j$  denoting the unit outward normal  
188 vector.

189 The implementation of the virtual work principle follow a procedure sim-  
190 ilar to the one suggested by Nielsen and Niordson (2012a) for an isotropic  
191 visco-plastic steady-state model with the exception that kinematic relations  
192 for a single crystalline material is employed here. This implementation pro-  
193 cedure also slightly deviate from the work of Dean and Hutchinson (1980),  
194 as this is a time dependent model. For a time dependent model, the his-  
195 tory dependence will enter through the plastic strain instead of through the  
196 stresses as in the original procedure (the plastic strains are streamline in-  
197 tegrated rather than the stresses). The virtual work principle in Eq. (6)  
198 has been discretized using a quadratic 8-node isoparametric element with re-  
199 duced Gauss integration ( $2 \times 2$  Gauss points). The pseudo algorithm for the  
200 rate-sensitive steady-state procedure in single crystals is as follows ( $n$  refers  
201 to the iterative step):

- 202 1. The plastic strain from the previous iteration,  $\varepsilon_{ij}^{p(n-1)}$ , is used to deter-  
203 mine the current displacement field,  $u_i^{(n)}$ , from the principle of virtual  
204 work in Eq. (6).
- 205 2. The total strain,  $\varepsilon_{ij}^{(n)}$ , is determined based on the displacement field,  
206  $u_i^{(n)}$ .

207 3. The slip and plastic strain fields are determined by the streamline in-  
208 tegration procedure.

- (a) First the spatial derivative of the slip (on the individual slip planes) and total plastic strains are determined by utilizing the steady-state relation ( $\partial f / \partial x_1 = -\dot{f} / \dot{a}$ )

$$\frac{\partial \gamma^{(\alpha)}}{\partial x_1} = -\frac{\dot{\gamma}_0}{\dot{a}} \text{sgn}(\tau^{(\alpha)}) \left( \frac{|\tau^{(\alpha)}|}{g^{(\alpha)}} \right)^{1/m} \quad (7)$$

$$\frac{\partial \varepsilon_{ij}^p}{\partial x_1} = \sum_{\alpha} \frac{\partial \gamma^{(\alpha)}}{\partial x_1} P_{ij}^{(\alpha)} \quad (8)$$

- 209 (b) Secondly, the current slip  $\gamma^{(\alpha)(n)}$  on each system and the current  
210 plastic strains,  $\varepsilon_{ij}^{p(n)}$ , are determined from the spatial derivatives  
211 by performing the streamline integration

$$\gamma^{(\alpha)(n)} = \int_{x_1^0}^{x_1^*} \frac{\partial \gamma^{(\alpha)}}{\partial x_1} dx_1, \quad \text{and} \quad \varepsilon_{ij}^{p(n)} = \int_{x_1^0}^{x_1^*} \frac{\partial \varepsilon_{ij}^p}{\partial x_1} dx_1. \quad (9)$$

- 212 4. The current stress field  $\sigma_{ij}^{(n)}$  is determined using the elastic constitutive  
213 relation.  
214 5. Step 1 through 4 is repeated by feeding the newly found plastic strain  
215 into the right hand side of the PWV in Eq. (6) until convergence is  
216 obtained.

217 The iterative procedure is initiated by using the purely elastic solution  
218 to the problem i.e.  $\gamma^{(\alpha)} = 0$  for the first step. The numerical stability of the  
219 steady-state algorithm has been found to be very sensitive to various param-  
220 eters, and especially for low rate-sensitivity exponents,  $m$ , difficulties with  
221 obtaining convergence is encountered. In order to improve the numerical sta-  
222 bility of the algorithm, changes have been made to the original procedure by  
223 Dean and Hutchinson (1980). The changes follow the suggestion by Niord-  
224 son (2001) and Nielsen and Niordson (2012a), where subincrement between  
225 Gauss points are introduced in the streamline procedure.

226 The steady-state model for single crystals has proven difficult to validate  
227 as limited literature exists on the topic. Thus, besides comparing to the ana-  
228 lytical and numerical results of Rice (1987); Rice et al. (1990), the model has

229 been compared to a strict plane strain isotropic model developed separately.  
 230 By systematically adding more slip systems a field matching the isotropic  
 231 model prediction was achieved.

### 232 3.3. The SSV model

233 Suo et al. (1993) presented a framework (the SSV-model) for cleavage  
 234 cracking surrounded by pre-existing dislocations. This model has been cho-  
 235 sen as it offers a simple and very robust method to evaluate the crack tip  
 236 shielding. The SSV-model is based on the assumption that no dislocations  
 237 are emitted from the crack front. This statement requires that the disloca-  
 238 tion spacing is much larger than the lattice constant, whereby the probability  
 239 for a pre-existing dislocation to blunt a major part of the crack tip is minor.  
 240 When no dislocations are emitted from the crack tip, the crack will propa-  
 241 gate by atomic separation, and thereby remain infinity sharp. Within this  
 242 region, where no dislocations are present, the material will therefore behave  
 243 elastically. When relating this to the numerical steady-state procedure, this  
 244 means that the crack is embedded within a thin material strip of height  $2D$   
 245 (see Fig. 1), which behaves elastically (the influence of the SSV domain ge-  
 246 ometry is investigated in Tvergaard, 1997). As the crack tip is embedded  
 247 in an elastic zone, linear elastic fracture mechanics applies, and the energy  
 248 release rate can be evaluated by the J-integral following the procedure of  
 249 Shih et al. (1986). When applying the J-integral (within the elastic SSV  
 250 domain), the corresponding fracture criterion is  $J_{tip} = \Gamma_{tip}$ , where  $\Gamma_{tip}$  de-  
 251 notes the energy release rate required for the crack to advance. It should be  
 252 mentioned that the SSV-model is not valid if the length of the separation  
 253 zone at the crack tip becomes comparable to the magnitude of the elastic  
 254 strip,  $D$ . Thus, the SSV-model is only valid for materials in which fracture  
 255 is dominated by cleavage or atomic separation (see detailed discussion in  
 256 e.g. Wei and Hutchinson, 1999). The height of the SSV domain can either  
 257 be regarded as a material fitting parameter (Suo et al., 1993) or it can be  
 258 estimated using dislocation theory (Beltz et al., 1996; Lipkin et al., 1996).

Based on the problem presented in Section 2, the crack tip shielding  
 ratio,  $J_{ss}/J_{tip}$ , is governed by the dimensional analysis conducted by Wei  
 and Hutchinson (1999), where  $J_{ss}$  is the remotely applied energy release  
 rate. This dimensional analysis states that the shielding ratio at steady-

state is given by

$$\frac{J_{ss}}{J_{tip}} = F \left( \frac{\dot{a}}{R_0 \dot{\gamma}_0}, \frac{R_0}{D}, \frac{\tau_0}{G}, N, m, \nu \right) \quad (10)$$

where the quantity  $\dot{a}/(R_0 \dot{\gamma}_0)$  will be denoted  $\zeta$ , to represent a dimensionless velocity. The parameter groups identified in Eq. (10) are therefore of key interest in developing a parametric understanding of crack growth in single crystals.

## 4. Results

The mesh employed in the model contains 102400 elements and is gradually scaled in two directions to obtain a very fine mesh in the vicinity of the crack tip where details are required. Approximately 19000 of the 102400 elements are concentrated within a region comparable to the plastic zone size in order to give a detailed solution.

### 4.1. Active Plastic Zones in Single Crystals

The first part of the results concerns the active plastic zone in the vicinity of the crack tip. These fields have previously been studied by Rice (1987) and Rice et al. (1990) for quasi-static crack growth, both analytically and numerically. In Rice (1987), analytical results showed that distinct zones, involving unloading and reloading to the yield point, takes place in the vicinity of the crack tip (see Fig. 4). These zones are seen as angular sectors which are separated by discontinuities in the velocity field at very specific locations related to the crystal orientation. The angles separating the sectors are characterized by being either perpendicular or parallel to the slip systems. The original analysis by Rice (1987) relies on perfectly plastic material behaviour ( $N \rightarrow 0$ ), in the rate-independent limit ( $m \rightarrow 0$ ), under Mode I loading condition. Rice (1987) presented analytical results for crack growth in the [101] direction with the crack plane orthogonal to the [010] direction, for both the FCC and BCC crystal structures. These crystal structures prove to have the same angular locations of the discontinuities since the effective slip systems in FCC and BCC crystal structures are perpendicular to each other.

In a later study, Rice et al. (1990) conducted a numerical investigation of the FCC structure in a quasi-static setting, validating the analytical results, by analysing the near tip plastic zone of a propagating crack. Direct comparison to the numerical results of Rice et al. (1990), is unfortunately not

290 possible as the propagation velocity in that particular analysis is unknown.  
 291 Despite this, the results can still be compared qualitatively. To improve on  
 292 these early results and bring out the effect of rate-sensitivity, the active plas-  
 293 tic zones for steady-state growth is presented in Figs. 5, 6, and 7 for FCC,  
 294 BCC, and HCP crystal structures, respectively. Here, the zones are shown  
 295 for different rate-sensitivity exponents,  $m$ , and a constant growth velocity of  
 296  $\zeta = \dot{a}/(R_0\dot{\gamma}_0) = 1000$ . The criterion for plasticity in the vicinity of the crack  
 297 tip has been adopted from Rice et al. (1990), and it is based on the accu-  
 298 mulated slip ( $\dot{\Lambda} = \sum_{\alpha} |\dot{\gamma}^{\alpha}|$ ). However, it should be mentioned that in the  
 299 results of Rice et al. (1990),  $\dot{\Lambda}$  is normalized by  $\tau_0/G$ , whereas here it is nor-  
 300 malized by  $\zeta\dot{\gamma}_0\tau_0/G$  in order to obtain non-dimensionality and comparable  
 301 fields across a large velocity span.

302 In contrast to Rice et al. (1990), who relied on a crack growing transiently  
 303 until it reaches steady-state, the results in Figs. 5-7 provide detailed steady-  
 304 state results for the plastic zone. Moreover, the purpose build framework  
 305 allows the computational effort to be focused on the crack tip such that  
 306 highly refined discretization can be employed. Comparing the findings of  
 307 Rice et al. (1990) (numerical results for the FCC crystal), to the results  
 308 presented in Fig. 5a reveals a striking match. Similar features, consisting  
 309 of two large active plastic features,  $\textcircled{B}$  and  $\textcircled{D}$ , and a plastic wake,  $\textcircled{A}$ ,  
 310 are observed. The expected velocity discontinuities illustrated by the white  
 311 regions (zones of largely concentrated plastic straining), correspond to the  
 312 prediction by Rice (1987) (see Fig. 4) with discontinuities at  $54.7^\circ$  and  
 313  $125.3^\circ$  and moreover, the size of the plastic features are of the same order  
 314 of magnitude. The plastic feature denoted  $\textcircled{B}$  is, however, somewhat longer  
 315 compared to feature  $\textcircled{D}$  in the present results. One possible explanation of  
 316 this could be that the solution in Rice et al. (1990), remains to fully reach  
 317 the steady-state. In their corresponding field for a stationary crack, Rice  
 318 et al. (1990) demonstrates a much different appearance of features  $\textcircled{B}$  and  
 319  $\textcircled{D}$  (where feature  $\textcircled{B}$  is almost absent), thus the features will have to evolve  
 320 significantly and become constant before the steady-state is reached. Another  
 321 significant difference between the two studies is the level of refinement as the  
 322 adopted steady-state approach allows focusing the discretization. E.g. both  
 323 the feature  $\textcircled{C}$  and protrusion on the leading edge of feature  $\textcircled{D}$  (vaguely  
 324 visible in Rice et al., 1990) stands out very clearly. By increasing the rate-  
 325 sensitivity (see Fig. 5b), the active plastic zones increases in size, however,  
 326 their characteristics remain similar, with the exception that the inclination of

feature (B) seems to be diminishing with increasing rate-sensitivity exponent,  $m$  (both for slowly and fast growing cracks).

Figure 6 presents similar, but new, results for the BCC crystal structure. Nowhere is a numerical comparison basis found, but according to Rice (1987), identical regions and velocity discontinuities, as for the FCC crystal, should be observed in the BCC crystal. This is confirmed in Fig. 6a for low rate-sensitivity exponent,  $m$ . Comparing the active plastic region for the FCC and BCC cases reveal large similarities, however, the two active plastic features, (B) and (D), are slightly larger for the BCC structure, while the wake, (A), is approximately the same size. The difference in magnitude can be explained by the effective slip systems found in Tab. 2. Only the  $90^\circ$  plane in a BCC crystal is an effective plane which has higher effective resistance to slip due to the scaling from Eq. (3). On the other hand, all planes for the FCC crystal are effective planes and thereby get a higher effective resistance to slip, resulting in a smaller plastic zone. Besides the difference in magnitude, the development of the small active plastic feature at (C) is not seen for the BCC crystal structure at low rate-sensitivity. However, at larger rate-sensitivity, this feature becomes evident and a larger similarity to results for the FCC crystal structure shows (compare Figs. 5b and 6b).

Lastly, the results for an HCP crystal structure is presented in Fig. 7. The results for the HCP crystal show a very different magnitude of the active plastic zones compared to both the FCC and BCC crystals. Comparing the results for low rate-sensitivity exponent,  $m$ , in Fig. 7a to the corresponding FCC crystal results (Fig. 5a), the feature (C) has now become much more dominant and the wake, (A), has also increased significantly in magnitude. As for the difference between the FCC and BCC crystals, the change in the plastic zone for the HCP crystal is tied to the corrections of the slip systems according to Eq. (3) (or the lack hereof). The HCP crystal structure has three active slip systems in the 2D plane meaning that creating effective systems are not needed and thus no corrections on the slip systems are imposed. Unfortunately, analytical results are yet to be developed for the HCP crystal structure, and a basis for comparison is missing. However, from the findings in Fig. 7a it is seen that the location of the velocity discontinuities obeys the conditions of being either perpendicular or parallel to the slip systems (as for both FCC and BCC crystals). When comparing to the discontinuities of the FCC and BCC crystals, an additional discontinuity is seen at feature (C), while the features (B) and (D) are closer together (smaller angle

364 between discontinuities) due to the  $60^\circ$  angle between active planes in the  
 365 HCP crystal.

366 By increasing the rate-sensitivity exponent,  $m$ , the active plastic zones  
 367 grow, just as for FCC and BCC crystals. However, due to the existence of  
 368 the more significant plastic feature  $\odot$ , the three zones which stay disjunct  
 369 for low rate-sensitivity now merge into one (the same tendency is expected  
 370 for FCC and BCC crystals, however, a larger rate-sensitivity exponent,  $m$ ,  
 371 would be required). Common for all crystals are that changes in the velocity  
 372 influence the magnitude of the plastic zone, but the proportions between the  
 373 individual features remain largely unchanged.

#### 374 4.2. Crack Tip Shielding Ratio in Single Crystals

375 The SSV-model is now introduced to investigate the shielding effect of the  
 376 plastic zones for the individual crystal structures. The following studies are  
 377 conducted under what is referred to as fast and slow crack growth, where the  
 378 dimensionless crack velocity is  $\zeta = 1000$  and  $\zeta = 10$ , respectively (recall that  
 379  $\zeta = \dot{a}/(R_0\dot{\gamma}_0)$ ). It should be noted that the fast growing crack is not reaching  
 380 velocities where dynamic effects become important and thus it can still be  
 381 handled as quasi-static crack growth where inertia effects are neglected.

382 Figure 8 presents the shielding ratio as a function of the height of the  
 383 elastic (dislocation free) SSV-region for both a slowly (Fig. 8a) and a fast  
 384 (Fig. 8b) growing crack under Mode I loading. Here, displaying results for  
 385 the both FCC, BCC, and HCP crystal structures. Common for both the fast  
 386 and slowly growing crack, in all crystal structures, is the increase in crack tip  
 387 shielding as the SSV region becomes thinner ( $R_0/D$  increases). Comparing  
 388 the three different crystal structures it is found that the largest shielding ratio  
 389 occurs for HCP crystals, while the lowest is found for FCC crystals. This is  
 390 in good agreement with the correction parameters stated in Tab. 2, where  
 391 the FCC crystal structure will exhibit the largest resistance against plastic  
 392 deformation and thereby the smallest plastic zone to shield the crack tip. In  
 393 contrast, the HCP crystal has the lowest resistance (no correction imposed,  
 394 as effective systems are not required), and thereby a large plastic zone, that  
 395 gives rise to a large shielding effect (consistent with previous observations  
 396 in Figs. 5, 6, and 7). The BCC crystal structure has only one effective slip  
 397 system, providing additional resistance, and therefore exhibits a crack tip  
 398 shielding between the FCC and HCP crystal.

399 The effect of varying the hardening exponent,  $N$ , for a constant rate-  
 400 sensitivity exponent,  $m$ , is brought out in Fig. 9. Here, a limited difference

between the slow and fast cracks is found since the rate-sensitivity exponent,  $m$ , is maintained fairly low. Regardless of the crack velocity, the same tendency as previously observed, regarding the highest shielding ratio for HCP crystals and the lowest for FCC crystals, still holds. For both the slow (Fig. 9a) and the fast crack (Fig. 9b) a decreasing hardening exponent,  $N$ , results in an increasing crack tip shielding due to more plastic deformation.

Another interesting observation, when comparing the fast and slowly growing cracks, regardless of the crystal structure, is the influence of the rate-sensitivity on the shielding ratio. For the slowly growing crack (Fig. 8a), the shielding is monotonically increasing with increasing rate-sensitivity exponent,  $m$ , while the opposite effect of a monotonically decreasing shielding is seen for the fast growing crack (Fig. 8b). The monotonic increase (decrease), for the low (high) velocity, naturally implies that the lines for different rate-sensitivities must intersect at one uniquely defined velocity (in accordance with the findings of Nielsen and Niordson (2012a) for isotropic materials). This behaviour is related to the rate dependency introduced through Eq (5) and it is not specific to isotropic nor single crystalline materials. The phenomenon can be explained by the same statement as Nielsen and Niordson (2012a) put forward which is based on the time aspect of the rate-sensitive model. Stress build-up or relaxation of the material occurs in the vicinity of the crack tip depending on the combination of velocity and rate-sensitivity. At low velocities, the material is given time to relax during the crack growth resulting in larger plastic strains i.e. more plastic dissipation and thus a larger shielding. In the opposite case where high velocities prevail, the relaxation is limited and leads to higher stresses (less plasticity) in the vicinity of the crack tip and thus lower shielding. This behaviour is largely dependent on the rate-sensitivity exponent,  $m$ , which will make the effect more or less pronounced.

To investigate the phenomena of a characteristic velocity, the uniquely defined intersection of the curves is further investigated in Fig. 10, where the shielding ratio is displayed as function of the dimensionless velocity,  $\zeta = \dot{a}/(R_0\dot{\gamma}_0)$ , for all three crystal structures. Clearly, it is common for all that a characteristic crack growth velocity exists (for fixed height of the SSV domain,  $R_0/D$ , and hardening exponent,  $N$ ), at which the shielding becomes independent of the rate-sensitivity exponent,  $m$ . This despite that the plastic zones may vary for different rate-sensitivities at this velocity. The existence of this characteristic velocity, however, opens up for the possibility of studying the rate-independent response using a rate-dependent model (see



also discussion in Nielsen et al., 2012b).

From Fig. 10 it is noticed that the characteristic velocity for the BCC and HCP crystals are very close, with the BCC crystal having a slightly larger value, whereas the characteristic velocity for the FCC crystal is significantly larger. Moreover, it is worth mentioning that the characteristic velocity for the HCP crystal in Fig. 10a (low hardening), is slightly off compared to the intersection in Fig. 10b (high hardening). A less distinct intersection of the curves is generally observed when the amount of plasticity is increasing in the problem as the large plastic zone tends to give difficulties in obtaining convergence.

## 5. Concluding Remarks

The active plastic zone that travels with a steadily growing crack in various single crystals have been analysed in detail. The crack is modelled in a steady-state framework where it is subject to Mode I loading in a rate-sensitive material setting. In accordance with Rice (1987), distinct sectors that divide the domain near the crack tip have been identified for the three most commonly encountered crystal structures in metals (FCC, BCC, and HCP). The size and shape of the plastic zone significantly affect the macroscopic fracture toughness of the material (the crack tip shielding ratio) as investigated by applying the SSV model (Suo et al., 1993). The main focus is on the effect of rate-sensitivity as-well as the effect of changing the crystal structures. The key findings are:

- Numerical simulation of single crystal indeed reveal discontinuities corresponding to the analytical results of Rice (1987), which are either perpendicular or parallel to the slip systems. Comparing results for low and high rate-sensitivity reveals that the active plastic zone changes in size, but the characteristics remain largely unchanged. The active plastic zone is very similar for the FCC and BCC crystal structures, while the HCP crystal structure differs substantially. This is linked to the scaling factors that affect plastic flow on the effective slip systems in the adopted 2D plane strain setting. The magnitude of the active plastic zone is smallest for the FCC crystal and largest for the HCP crystal.
- The shielding ratio is smallest for the FCC crystal and largest for the HCP crystal, consistent with the magnitude of the plastic zones for

the two different crystal structures. Generally, the shielding ratio is observed to increase with  $R_0/D$ . As  $R_0/D$  increases, the SSV domain decreases in height, which in turn result in more plastic dissipation that contributes to the crack tip shielding. The shielding ratio also increases for a decreasing hardening exponent,  $N$ , by the same argument, namely that the plastic dissipation is increasing.

- At low velocities, increasing rate-sensitivity leads to a monotonically increasing crack tip shielding ratio, whereas the opposite is observed for high velocities. This monotonically increase/decrease in the response lead to the finding of a characteristic velocity at which the shielding ratio becomes independent of the rate-sensitivity. The BCC and HCP crystal structures are found to have similar characteristic velocities (the BCC structure is slightly larger than the HCP structure), whereas the FCC crystal structure has a significantly larger characteristic velocity.

## 6. Acknowledgement

The work is financially supported by The Danish Council for Independent Research in the project “New Advances in Steady-State Engineering Techniques”, grant DFF-4184-00122. Ph.D Chris Valentin Nielsen, DTU Mechanical Engineering, is greatly acknowledged for his parallelization of the skyline solver module (Nielsen et al., 2012).

494 **References**

- 495 Anderson, T. L., 2005. Fracture Mechanics: Fundamentals and Applications,  
496 Third Edition. Taylor and Francis.
- 497 Beltz, G. E., Rice, J. R., Shih, C. F., Xia, L., 1996. A self-consistent model  
498 for cleavage in the presence of plastic flow. *Acta Materialia* 44, 3943–3954.
- 499 Dahlberg, C. F. O., Saito, Y., Öztop, M. S., Kysar, J. W., 2014. Geometri-  
500 cally necessary dislocation density measurements associated with different  
501 angles of indentations. *Int. J. Plas.* 54, 81–95.
- 502 Dean, R. H., Hutchinson, J. W., 1980. Quasi-static steady crack growth  
503 in small-scale yielding. *Fracture Mechanics: Twelfth Conference, ASTM*  
504 *STP700*, American Society for Testing and Materials, 383–405.
- 505 Hui, C. Y., 1983. Steady-state crack growth in elastic power-law creeping  
506 materials. In: *elastic-plastic fracture: second symposium. Inelastic crack*  
507 *analysis, ASTM STP803*, vol. 1, American Society for Testing and Mate-  
508 *rials*, 573–93.
- 509 Hutchinson, J. W., 1976. Bounds and self-consistent estimates for creep of  
510 polycrystalline materials. *Proc. R. Soc. Lond. A* 348, 101–127.
- 511 Juul, K. J., Nielsen, K. L., Niordson, C. F., 2017. Steady-state numerical  
512 modeling of size effects in micron scale wire drawing. *J. Manuf. Process.*  
513 25, 163–171.
- 514 Kysar, J. W., Gan, Y. X., Mendez-Arzuza, G., 2005. Cylindrical void in  
515 a rigid-ideally plastic single crystal. Part I: Anisotropic slip line theory  
516 solution for face-centered cubic crystals. *Int. J. Plas.* 21, 1481–1520.
- 517 Lipkin, D. M., Clarke, D. R., Beltz, G. E., 1996. A strain-gradient model  
518 of cleavage fracture in plastically deforming materials. *Acta Materialia* 44,  
519 4051–4058.
- 520 Nielsen, C. V., Zhang, W., Alves, L. M., Bay, N., Martins, P. A. F., 2012.  
521 *Modeling of Thermo-Electro-Mechanical Manufacturing Processes with*  
522 *Applications in Metal Forming and Resistance Welding*, First Edition.  
523 Springer.

524 Nielsen, K. L., Niordson, C. F., 2012a. Rate sensitivity of mixed mode in-  
 525     interface toughness of dissimilar metallic materials: Studied at steady state.  
 526     Int. J. Solids Struct. 49, 576–583.

527 Nielsen, K. L., Niordson, C. F., Hutchinson, J. W., 2012b. Strain gradient ef-  
 528     fects on steady-state crack growth in rate-dependent materials. Eng. Fract.  
 529     Mech. 96, 61–71.

530 Niordson, C. F., 2001. Analysis of steady-state ductile crack growth along a  
 531     laser weld. Int. J. Frac. 111, 53–69.

532 Niordson, C. F., Kysar, J. W., 2014. Computational strain gradient crystal  
 533     plasticity. J. Mech. Phys. Solids 62, 31–47.

534 Ortiz, M., Mohan, R., Shih, C. F., 1992. An analysis of cracks in ductile  
 535     single crystals-II. Mode I loading. J. Mech. Phys. Solids 40, 315–337.

536 Rice, J. R., 1987. Tensile crack tip fields in elastic-ideally plastic crystals.  
 537     Mech. Mater. 6, 317–335.

538 Rice, J. R., Hawk, D. E., Asaro, R. J., 1990. Crack tip fields in ductile  
 539     crystals. Int. J. Frac. 42, 301–322.

540 Roberts, S. G., Hirsch, P. B., Booth, A. S., Ellis, M., Serbena, F. C., 1993.  
 541     Dislocations, cracks and brittleness in single crystals. Phys. Scripta T49,  
 542     420–426.

543 Shih, C. F., Moran, B., Nakamura, T., 1986. Energy release rate along a  
 544     three-dimensional crack front in a thermally stressed body. Int. J. Frac.  
 545     30, 79–102.

546 Suo, Z., Shih, C. F., Varias, A. G., 1993. A theory for cleavage cracking in  
 547     the presence of plastic flow. Acta Metall Mater 41, 1551–7.

548 Tarleton, E., Roberts, S. G., 2009. Dislocation dynamic modelling of the  
 549     brittle-ductile transition in tungsten. Phil. Mag. 89, 2759–2769.

550 Tvergaard, V., 1997. Cleavage crack growth resistance due to plastic flow  
 551     around a near-tip dislocation-free region. J. Mech. Phys. Solids 45, 1007–  
 552     23.

553 Wei, Y., Hutchinson, J. W., 1999. Models of interface separation accompa-  
 554     nied by plastic dissipation at multiple scales. Int. J. Frac. 95, 1–17.

## 555 List of Figures

556	1	Mode I crack growth at steady-state in rate-sensitive crystal plastic material. The SSV domain provide an elastic strip embedded in the steady-state domain (SS domain). The crack is loaded with an elastic $K_I$ far field. . . . .	22
557			
558			
559			
560	2	FCC and BCC crystal structure with the crack front along the $[10\bar{1}]$ direction in the (010) crack plane (Rice, 1987). . . . .	23
561			
562	3	Mode I crack growth in single crystal with three and four Miller indices representing FCC/BCC and HCP, respectively. The sharp crack front is along the $[10\bar{1}]/[0001]$ direction and the three effective slip systems are oriented as shown for FCC, BCC and HCP crystal structures. . . . .	24
563			
564			
565			
566			
567	4	Velocity discontinuities and angle of secondary plastic zone at a steadily moving crack tip creating angular sectors for FCC and BCC crystals according to Rice (1987). . . . .	25
568			
569			
570	5	Accumulated slip rate, $\dot{\Lambda}$ , for steady-state crack growth in perfectly plastic single crystal showing the plastic region, $\dot{\Lambda}G/(\zeta\dot{\gamma}_0\tau_0) \geq 1$ , (black region) and a region of highly concentrated plastic straining, $\dot{\Lambda}G/(\zeta\dot{\gamma}_0\tau_0) \geq 2000$ , (white region) in an FCC crystal for constant crack velocity $\zeta = 1000$ with (a) $m = 0.01$ , and (b) $m = 0.05$ . . . . .	26
571			
572			
573			
574			
575			
576	6	Accumulated slip rate, $\dot{\Lambda}$ , for steady-state crack growth in perfectly plastic single crystal showing the plastic region, $\dot{\Lambda}G/(\zeta\dot{\gamma}_0\tau_0) \geq 1$ , (black region) and a region of highly concentrated plastic straining, $\dot{\Lambda}G/(\zeta\dot{\gamma}_0\tau_0) \geq 2000$ , (white region) in a BCC crystal for constant crack velocity $\zeta = 1000$ with (a) $m = 0.01$ , and (b) $m = 0.05$ . . . . .	27
577			
578			
579			
580			
581			
582	7	Accumulated slip rate, $\dot{\Lambda}$ , for steady-state crack growth in perfectly plastic single crystal showing the plastic region, $\dot{\Lambda}G/(\zeta\dot{\gamma}_0\tau_0) \geq 1$ , (black region) and a region of highly concentrated plastic straining, $\dot{\Lambda}G/(\zeta\dot{\gamma}_0\tau_0) \geq 2000$ , (white region) in an HCP crystal for constant crack velocity $\zeta = 1000$ with (a) $m = 0.01$ , and (b) $m = 0.05$ . . . . .	28
583			
584			
585			
586			
587			
588	8	Crack tip shielding ratio vs. inverse of dislocation free region (SSV), $D$ , for single crystal with parameters; $N = 0.10$ and velocity (a) $\zeta = 10$ , and (b) $\zeta = 1000$ . . . . .	29
589			
590			

591	9	Crack tip shielding ratio vs. inverse of dislocation free region	
592		(SSV), $D$ , for single crystal with parameters; $m = 0.01$ and	
593		velocity (a) $\zeta = 10$ , and (b) $\zeta = 1000$ . . . . .	30
594	10	Crack tip shielding ratio as function of velocity for constant	
595		SSV domain size $R_0/D = 80$ with hardening exponent (a)	
596		$N = 0.10$ , and (b) $N = 0.20$ . . . . .	31

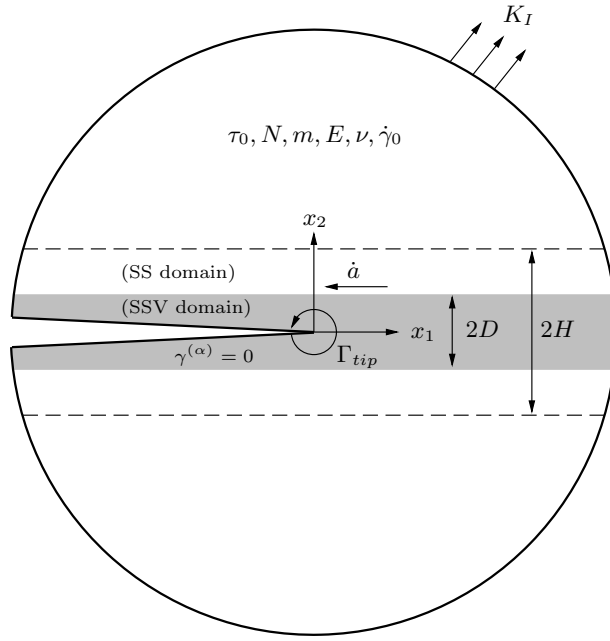


**Figure 1:** Mode I crack growth at steady-state in rate-sensitive crystal plastic material. The SSV domain provide an elastic strip embedded in the steady-state domain (SS domain). The crack is loaded with an elastic  $K_I$  far field.

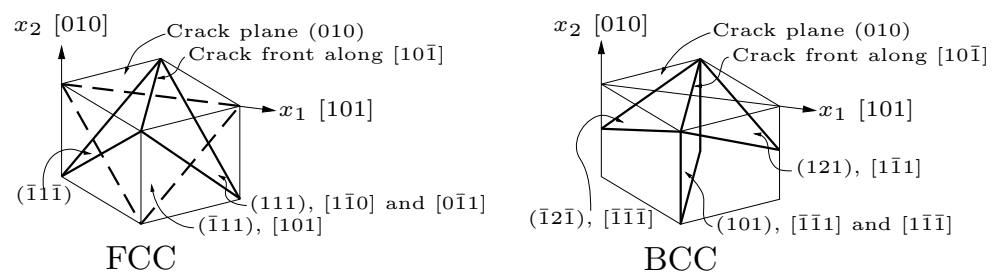


**Figure 2:** FCC and BCC crystal structure with the crack front along the  $[10\bar{1}]$  direction in the  $(010)$  crack plane (Rice, 1987).



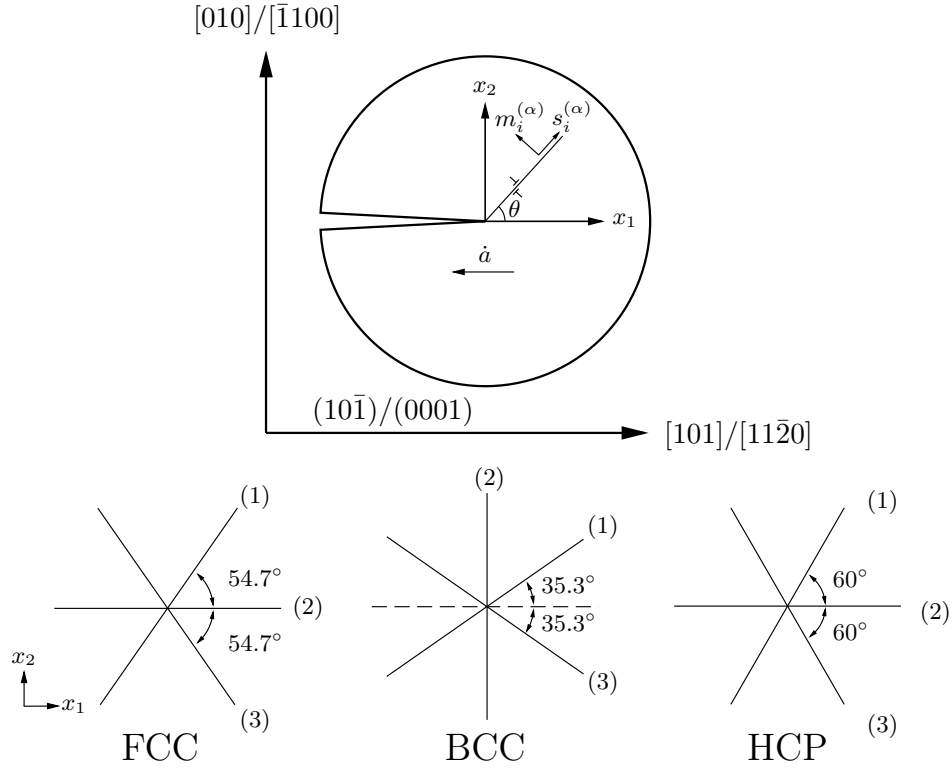


**Figure 3:** Mode I crack growth in single crystal with three and four Miller indices representing FCC/BCC and HCP, respectively. The sharp crack front is along the  $[10\bar{1}]/[0001]$  direction and the three effective slip systems are oriented as shown for FCC, BCC and HCP crystal structures.

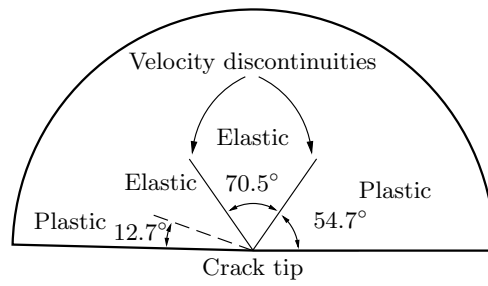


**Figure 4:** Velocity discontinuities and angle of secondary plastic zone at a steadily moving crack tip creating angular sectors for FCC and BCC crystals according to Rice (1987).

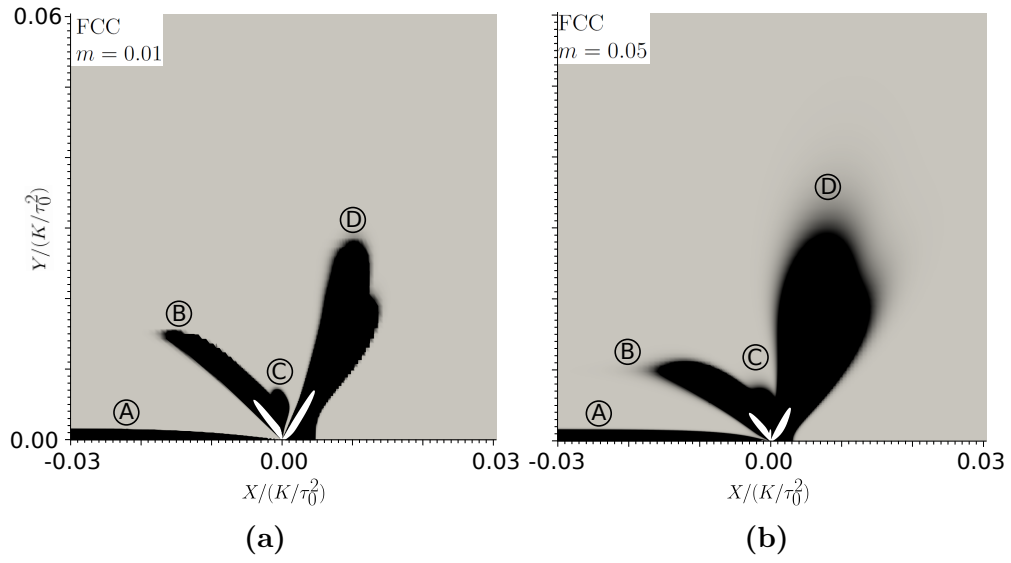


**Figure 5:** Accumulated slip rate,  $\dot{\Lambda}$ , for steady-state crack growth in perfectly plastic single crystal showing the plastic region,  $\dot{\Lambda}G/(\zeta\dot{\gamma}_0\tau_0) \geq 1$ , (black region) and a region of highly concentrated plastic straining,  $\dot{\Lambda}G/(\zeta\dot{\gamma}_0\tau_0) \geq 2000$ , (white region) in an FCC crystal for constant crack velocity  $\zeta = 1000$  with (a)  $m = 0.01$ , and (b)  $m = 0.05$ .

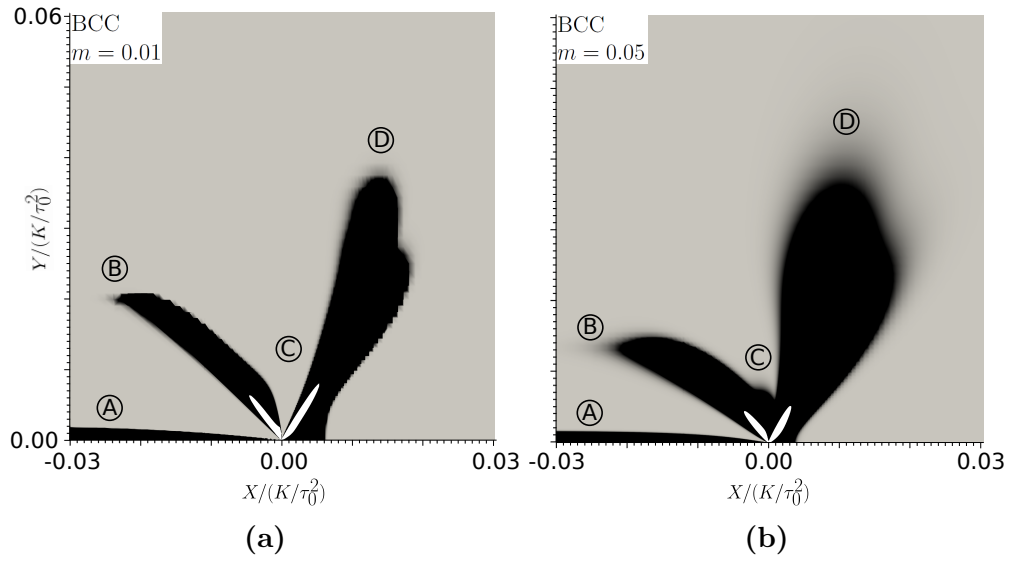


**Figure 6:** Accumulated slip rate,  $\dot{\Lambda}$ , for steady-state crack growth in perfectly plastic single crystal showing the plastic region,  $\dot{\Lambda}G/(\zeta\dot{\gamma}_0\tau_0) \geq 1$ , (black region) and a region of highly concentrated plastic straining,  $\dot{\Lambda}G/(\zeta\dot{\gamma}_0\tau_0) \geq 2000$ , (white region) in a BCC crystal for constant crack velocity  $\zeta = 1000$  with (a)  $m = 0.01$ , and (b)  $m = 0.05$ .

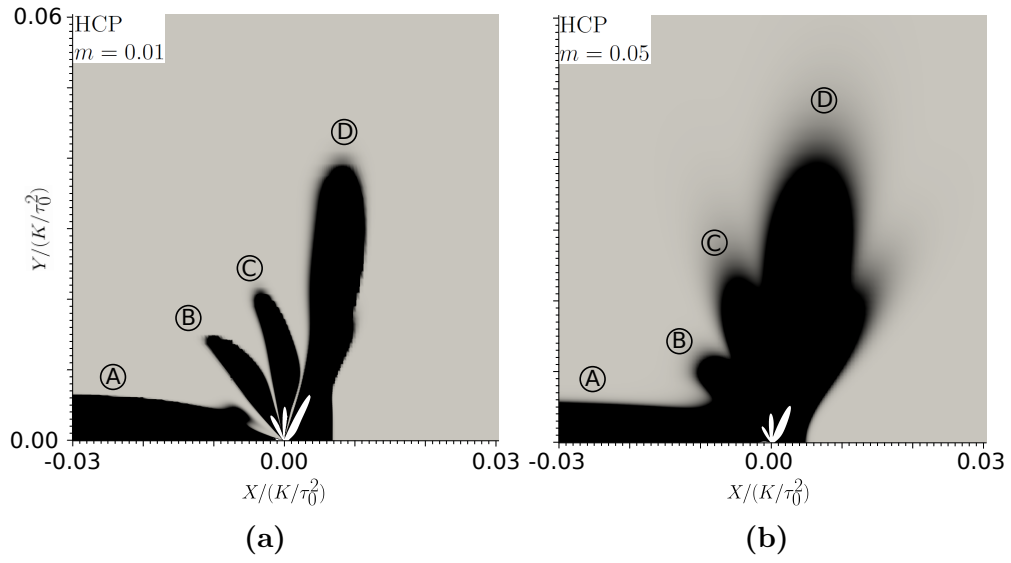
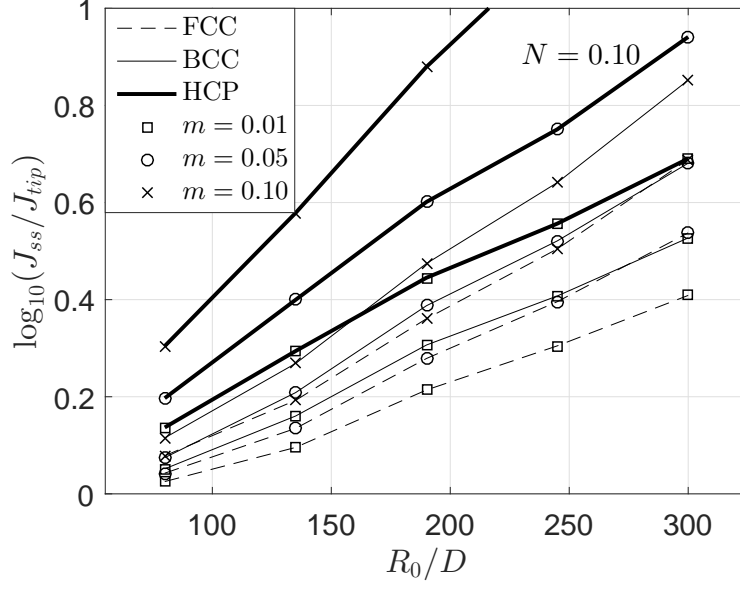
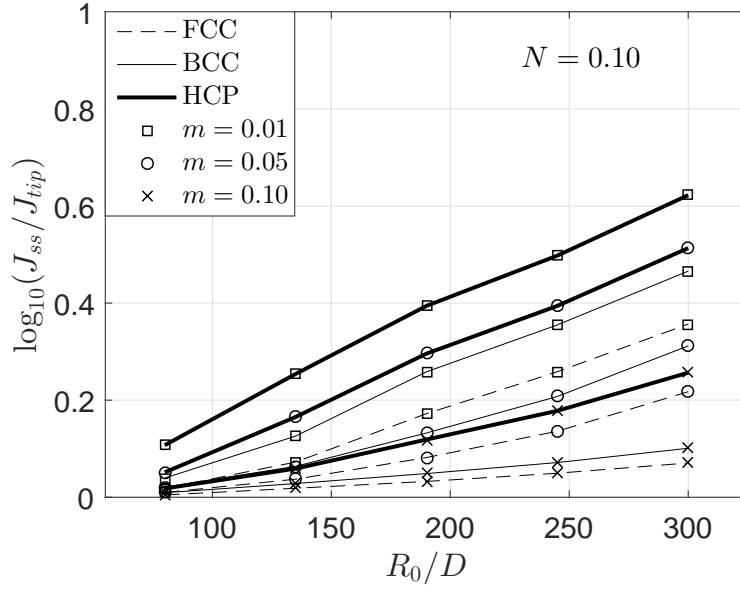


**Figure 7:** Accumulated slip rate,  $\dot{\Lambda}$ , for steady-state crack growth in perfectly plastic single crystal showing the plastic region,  $\dot{\Lambda}G/(\zeta\dot{\gamma}_0\tau_0) \geq 1$ , (black region) and a region of highly concentrated plastic straining,  $\dot{\Lambda}G/(\zeta\dot{\gamma}_0\tau_0) \geq 2000$ , (white region) in an HCP crystal for constant crack velocity  $\zeta = 1000$  with (a)  $m = 0.01$ , and (b)  $m = 0.05$ .

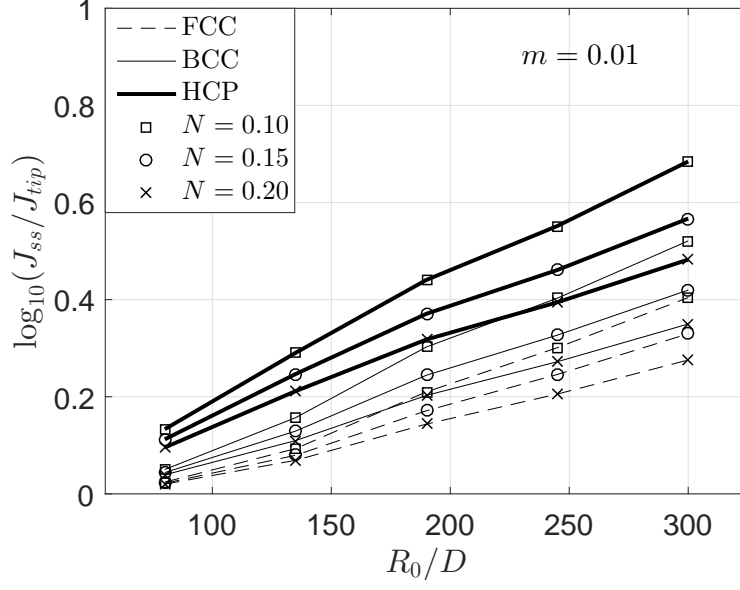


(a)

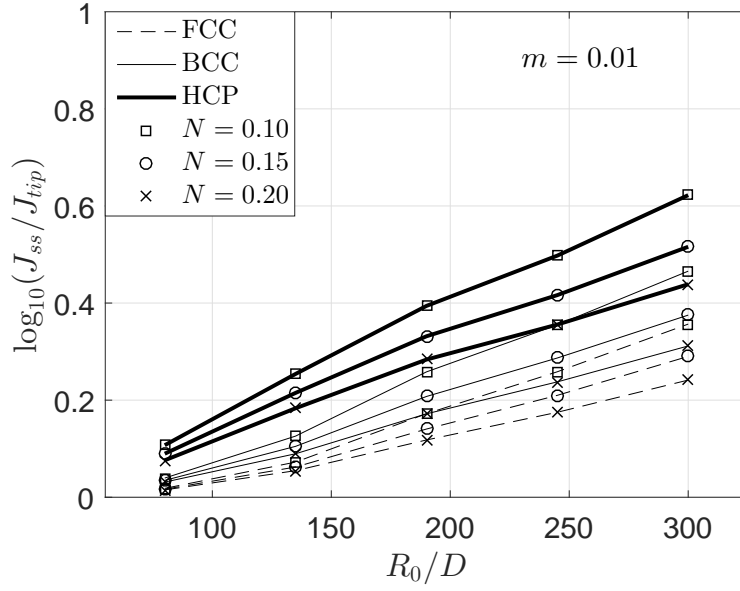


(b)

**Figure 8:** Crack tip shielding ratio vs. inverse of dislocation free region (SSV),  $D$ , for single crystal with parameters;  $N = 0.10$  and velocity (a)  $\zeta = 10$ , and (b)  $\zeta = 1000$ .



(a)



(b)

**Figure 9:** Crack tip shielding ratio vs. inverse of dislocation free region (SSV),  $D$ , for single crystal with parameters;  $m = 0.01$  and velocity (a)  $\zeta = 10$ , and (b)  $\zeta = 1000$ .

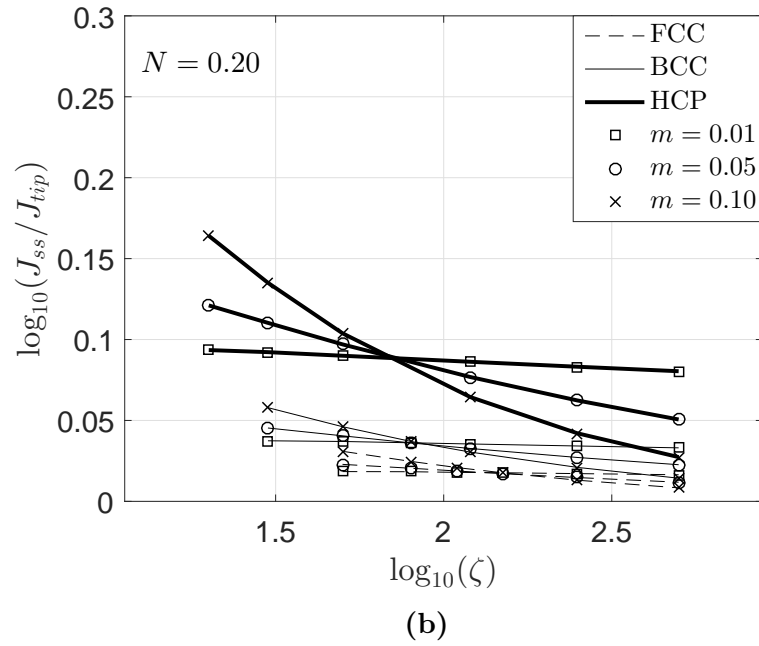
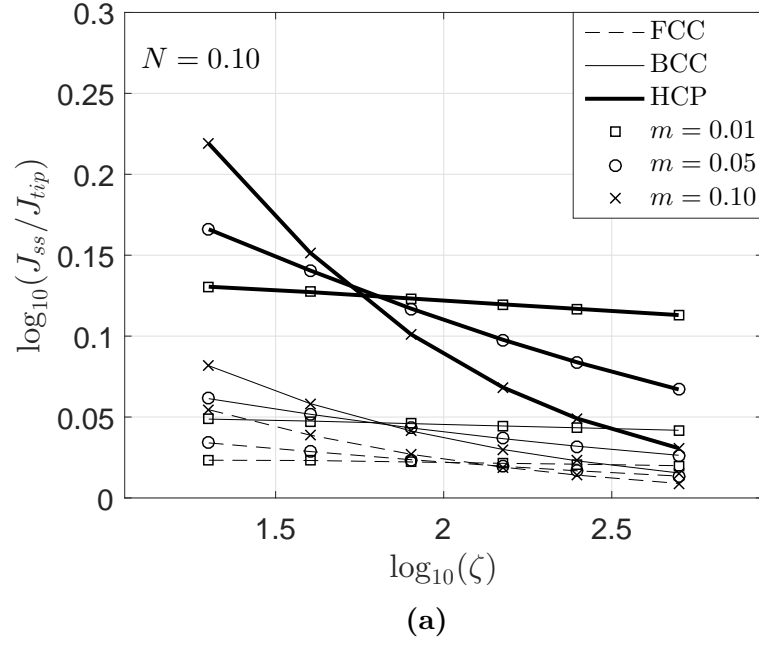


**Figure 10:** Crack tip shielding ratio as function of velocity for constant SSV domain size  $R_0/D = 80$  with hardening exponent (a)  $N = 0.10$ , and (b)  $N = 0.20$ .



597 **List of Tables**

598	1	Material properties. . . . .	33
599	2	Crystallographic slip systems and the corresponding effective	
600		slip systems. . . . .	34

Parameter	Significance	Value
$\tau_0/G$	Yield strain	0.001
$\nu$	Poisson ratio	0.3
$N$	Strain hardening exponent	0-0.2
$m$	Strain rate-sensitivity exponent	0.01-0.1
$\dot{\gamma}_0$	Reference slip rate	0.002
$\Gamma_{tip}$	Near tip fracture energy	1 J/m <sup>2</sup>

**Table 1:** Material properties.

Effective slip system no.	(1)	(2)	(3)
FCC crystal			
Angle to [101] in ( $\bar{1}01$ ) plane	54.7°	0°	-54.7°
Crystallographic slip system (a)	(111)[ $\bar{1}\bar{1}0$ ]	( $\bar{1}1\bar{1}$ )[101]	( $\bar{1}\bar{1}\bar{1}$ )[0 $\bar{1}\bar{1}$ ]
Crystallographic slip system (b)	(111)[0 $\bar{1}1$ ]	( $\bar{1}1\bar{1}$ )[101]	( $\bar{1}\bar{1}\bar{1}$ )[ $\bar{1}\bar{1}0$ ]
$\beta(\alpha) = \frac{s_i^{(\alpha a)}m_j^{(\alpha a)} + s_i^{(\alpha b)}m_j^{(\alpha b)}}{s_i^{(\alpha)}m_j^{(\alpha)}}$	$\sqrt{3}$	$\frac{2}{\sqrt{3}}$	$\sqrt{3}$
$\lambda(\alpha) = \frac{\tau^{(\alpha)}}{\tau^{(\alpha a)}} = \frac{\tau^{(\alpha)}}{\tau^{(\alpha b)}}$	$\frac{2}{\sqrt{3}}$	$\sqrt{3}$	$\frac{2}{\sqrt{3}}$
BCC crystal			
Angle to [101] in ( $\bar{1}01$ ) plane [°]	35.3°	90°	-35.3°
Crystallographic slip system (a)	(121)[ $\bar{1}\bar{1}1$ ]	(101)[ $\bar{1}\bar{1}1$ ]	( $\bar{1}2\bar{1}$ )[ $\bar{1}\bar{1}\bar{1}$ ]
Crystallographic slip system (b)	-	(101)[ $\bar{1}\bar{1}\bar{1}$ ]	-
$\beta(\alpha) = \frac{s_i^{(\alpha a)}m_j^{(\alpha a)} + s_i^{(\alpha b)}m_j^{(\alpha b)}}{s_i^{(\alpha)}m_j^{(\alpha)}}$	1	$\frac{2}{\sqrt{3}}$	1
$\lambda(\alpha) = \frac{\tau^{(\alpha)}}{\tau^{(\alpha a)}} = \frac{\tau^{(\alpha)}}{\tau^{(\alpha b)}}$	1	$\sqrt{3}$	1
HCP crystal			
Angle to [11 $\bar{2}0$ ] in (0001) plane [°]	60°	0°	-60°
Crystallographic slip system (a)	(10 $\bar{1}0$ )[1 $\bar{2}10$ ]	( $\bar{1}\bar{1}00$ )[ $\bar{1}\bar{1}20$ ]	(01 $\bar{1}0$ )[2 $\bar{1}\bar{1}0$ ]
Crystallographic slip system (b)	-	-	-
$\beta(\alpha) = \frac{s_i^{(\alpha a)}m_j^{(\alpha a)} + s_i^{(\alpha b)}m_j^{(\alpha b)}}{s_i^{(\alpha)}m_j^{(\alpha)}}$	1	1	1
$\lambda(\alpha) = \frac{\tau^{(\alpha)}}{\tau^{(\alpha a)}} = \frac{\tau^{(\alpha)}}{\tau^{(\alpha b)}}$	1	1	1

**Table 2:** Crystallographic slip systems and the corresponding effective slip systems.